European Journal of Haematology ISSN 0902-4441

CASE REPORT

Epithelioid hemangioendothelioma presenting with severe myelofibrosis and a high serum hyaluronan level

Youko Suehiro[1], Yoshimichi Tachikawa[1], Yasunobu Abe[2], Koichi Ohshima[3], Koichiro Muta[2], Kenzaburo Tani[1]

[1]Department of Advanced Molecular and Cell Therapy, Kyushu University; [2]Department of Medicine and Bioregulatory Science, Graduate School of Medical Science, Kyushu University, Fukuoka, Japan; [3]Department of Pathology, School of Medicine, Kurume University, Kurume, Japan

Abstract

Epithelioid hemangioendothelioma (EHE) is a rare tumor originating from the vascular endothelium; it has an intermediate malignant potential. EHEs affect all age groups and mostly originate from the soft tissues of the extremities, lungs, and liver. Spinal EHEs, especially those occurring in the bone marrow region, are extremely rare. We report a case of EHE with massive involvement of the liver, vertebrae, and cranial bones that caused severe myelofibrosis (MF) in a 67-yr-old-male patient. Hyaluronan deposits were diffusely observed in the tumor tissue biopsies obtained from both the liver and bone marrow. Furthermore, the serum hyaluronan level increased markedly along with rapid progression of the disease. To the best of our knowledge, this is the first report of MF occurring in an EHE; hyaluronan may have played an important role in the pathogenesis of fibrosis in this case.

Key words epithelioid hemangioendothelioma; myelofibrosis; hyaluronan

Correspondence Youko Suehiro MD, PhD, Department of Advanced Molecular and Cell Therapy, Kyushu University, 3-1-1 Maidashi, Higashi-ku, Fukuoka 812-8582, Japan. Tel: +81 92 642 5996; Fax: +81 92 642 5997; e-mail: suehiro@sentan.med.kyushu-u.ac.jp

Accepted for publication 26 May 2007

doi:10.1111/j.1600-0609.2007.00909.x

Since epithelioid hemangioendothelioma (EHE) was first described as a soft-tissue neoplasm in 1982 by Weiss and Enzinger (1), it has been found to occur in many other sites, such as the lungs, liver, mediastinum, brain, and bone (2–7). In most cases, EHE occurs in a single organ. Multi-organ involvement occurs occasionally and reflects metastasis or multicentric disease. However, bone marrow involvement is extremely rare. We describe an EHE case with bone marrow involvement complicated by severe bone marrow fibrosis. To the best of our knowledge, this is the first reported case of bone marrow fibrosis caused by EHE infiltration.

Case report

A 67-yr-old man presented to his local hospital in May 2005, 4 months prior to admission to our hospital, with a chief complaint of purpura. He was diagnosed as having allergic purpura and treated with prednisolone. Anemia and an elevated C-reactive protein level found at that time continued for 3 months. A bone marrow examination was done, showing a dry tap; he was diagnosed and followed as having myelofibrosis (MF), although hepatosplenomegaly was not observed. Over time, the patient's symptoms, such as severe headache and back pain, as well as his anemia, continued, and his alkaline phosphatase (ALP) level increased progressively. He had no previous surgery, transfusions, or exposure to known hepatotoxins. There were histories of liver cirrhosis and hepatocellular carcinoma in his family. The patient was referred to the Hematology service of Kyushu University Hospital in September, 2005. The peripheral blood analysis revealed bicytopenia (Hb 7.9 g/dL, platelets 10.4×10^{10}/L), and a white blood cell count of 8.5×10^9/L with leukoerythroblastosis. The serum ALP (1195 U/L; normal range, 115–359 U/L) and serum hyaluronan (307 ng/mL; normal range < 50 ng/mL) levels were elevated. However, all hepatitis virus markers were negative, and tumor marker levels, including α-fetoprotein, carcinoembryonic antigen, and cancer antigen 19–9

levels, were normal. Bone marrow aspiration resulted in a dry tap, and the bone marrow biopsy showed fibrosis with marked hyalinization; normal hematopoiesis was severely suppressed (Fig. 1G). Silver stain showed an increase in reticulin fibers surrounding of the cellular components (data not shown). The JAK2 mutation, a gene abnormality that induces MF, was not detected in peripheral blood mononuclear cells. Thus, the patient was referred for further examination. On ultrasound (US) examination of the liver, multiple hypoechoic lesions were seen. Enhanced computed tomography (CT) scans showed multiple heterogeneous low-density masses in bilateral liver lobes (Fig. 2A). Positron emission tomography (PET) revealed heterogeneous FDG accumulation in the spine, pelvis, and femora, as well as a hot spot in S7 of the liver (Fig. 2C). Magnetic resonance imaging (MRI) examination of the spine and head showed heterogeneous high and moderately low signal intensity on T2-weighted images with gadolinium enhancement, suggesting progressive marrow replacement (Fig. 2D–F).

The patient had a liver biopsy and bone marrow biopsies from the iliac crest and spine (L3). Microscopically, the liver specimen showed invasive tumor lesions with a well-demarcated border that distinguished them from the surrounding normal liver tissue. The tumor consisted of spindle cells and signet ring cell-like structure with intracytoplasmic lumina. Epithelioid cells were medium to large, rounded in shape, and had an eosinophilic cytoplasm and vesicular nuclei (Fig. 1A,B). Immunohistochemical analysis of the tumor cells revealed focal staining for CD34 and cytokeratins (AE1/AE3), and weak staining for factor VIII-related antigen (Fig. 1D–F). The bone marrow specimens were found to have diffuse fibrosis with marked hyalinization change and no evidence of normal hematopoiesis (Fig. 1G,H). On immunohistochemistry, the bone marrow lesion consisted of spindle cells that were positive for CD34 and cytokeratins (AE1/AE3) and weakly positive for factor VIII-related antigen (Fig. 1J–L). These findings were entirely compatible with previous EHE reports. In addition, hyaluronan deposits were observed diffusely in the tumor

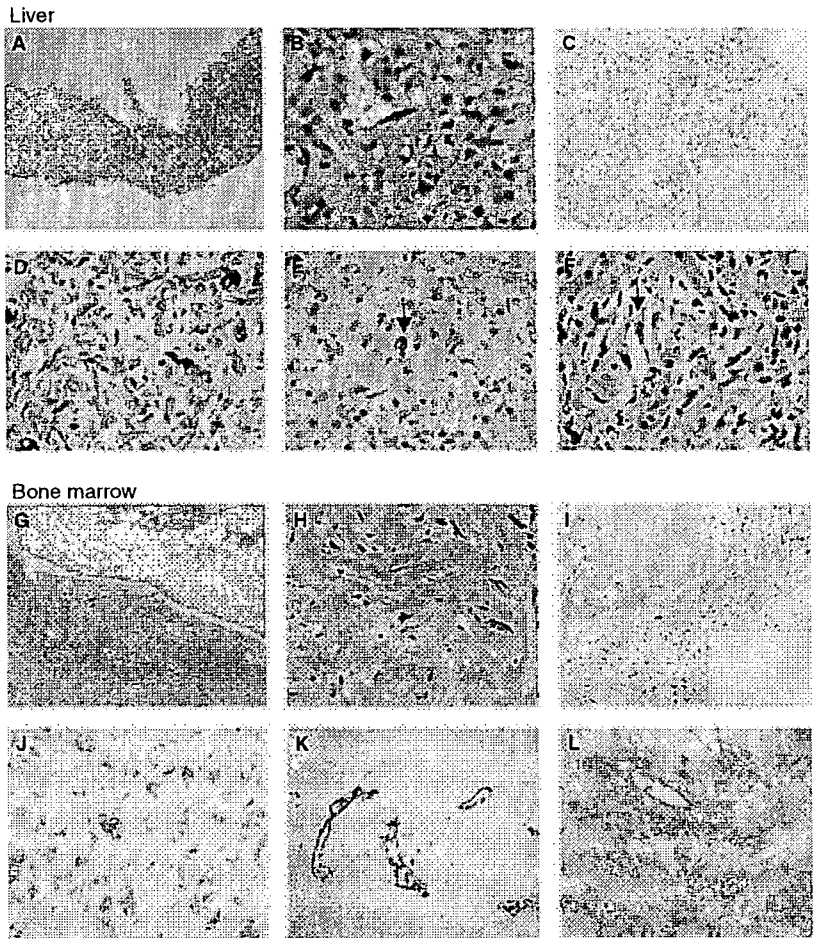

Figure 1 In the liver specimens (A–F), the invading tumor is well-demarcated from the surrounding hepatocytes. The tumor consists of spindle cells, signet ring cell-like structure with intracytoplasmic lumina (A, B: H&E); diffuse hyaluronan deposits are seen (C: alcian blue staining and hyaluronidase digestion). Bone marrow specimens (G–L) show diffuse fibrosis with marked hyaluronan deposits and no evidence of normal hematopoiesis (G, H: H&E, I: alcian blue staining and hyaluronidase digestion). Immunohistochemical analysis shows tumor tissue focally stained by cytokeratins (D, J) and CD34 (E, K), and weakly stained by factor VIII-related antigen (F, L). Magnifications are 100× (A, G), 200× (C, I) and 400× (B, D–F, H, J–L).

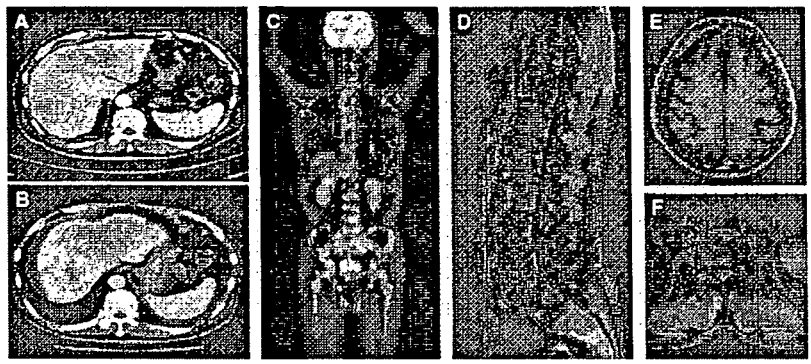

Figure 2 Computed tomography (CT) scan before chemotherapy shows heterogeneous low-density masses in bilateral liver lobes (A). On CT 2 months later, severe atrophy of the right liver lobe and an increase of the number and the size of multiple, bilateral masses is seen (B). FDG-PET shows heterogeneous FDG accumulation in the systemic spine, pelvis, and femora, as well as a hot spot in S7 of the liver (C). MRI examination of the spine and head shows heterogeneous intensity on T2-weighted images with gadolinium enhancement, suggesting progressive marrow replacement by the tumors (D–F).

tissues obtained from both the liver and bone marrow (Fig. 1C,I). The severe bone marrow fibrosis was likely because of EHE involvement. High levels of vascular endothelial growth factor (VEGF, 339 pg/mL) and transforming growth factor-β (TGF-β, 10.6 ng/mL) were noted at the time of diagnosis; these two factors likely promoted the fibrosis.

As surgery was not indicated because of the presence of multiple lesions, the patient was given chemotherapy with etoposide, carboplatin, and interferon-α 7 wk after admission. The ALP, VEGF (116 pg/mL), and TGF-β (3.31 ng/mL) level decreased after chemotherapy was started. However, the patient's headache and back pain became worse, and then, within 2 months of starting chemotherapy, the patient's liver dysfunction and pancytopenia were exacerbated, and his serum hyaluronan, a marker of liver cirrhosis, increased markedly (up to 28 900 ng/mL), along with an increase in his TGF-β level to 13.4 ng/mL. The CT done at the same time showed severe atrophy of the right liver lobe because of fibrosis and an increase in the number and size of the multiple masses located in bilateral hepatic lobes in only 4 wk (Fig. 2B). The patient died because of EHE 5 months after the diagnosis of MF.

Discussion

Bone marrow invasion or metastasis in EHE patients is extremely rare and difficult to diagnose. Only three such cases have been previously reported, as shown in Table 1 (8–10). Vertebral lesions were observed in all cases, and patients had multiple tumor locations. In all cases, bone marrow lesions were identified on imaging examinations such as MRI and FDG PET; this indicates that these imaging modalities are useful and essential for diagnosing bone marrow infiltration. The bone marrow was examined in cases 1, 2, and the present case. Only in the present case was diffuse fibrosis observed with abundant hyalinization; therefore, multiple bone marrow biopsies were required to provide sufficient tissue for establishing

Table 1 Clinical characteristics of bone marrow involvement in EHE cases

Case	Age/Gender	Symptoms	Laboratory data	Tumor location	Treatment	Survival
Case 1 (8)	45/M	Back pain, pleuritic chest pain	t(7;22), t(14;14)	Perispinous muscles, vertebrae, Lung, BM	Surgery, radiation	Dead (16 months)
Case 2 (9)	51/M	Fatigue, splenomegaly	Hb 6.5 g/dL, ALP↑	Liver, vertebrae, pelvis, BM	Splenectomy, chemotherapy	>14 months
Case 3 (10)	65/M	Shoulder, hip, sternum pain	CRP 11.8 mg/dL, FDG-PET+	Mediastinal LNs, lung, vertebrae, BM	Chemotherapy, radiation	Dead (14 months)
Present case	67/M	Headache, back pain, fatigue	Hb 7.9 g/dL, Plt10.4 × 10^{10}/L, CRP 6.7 mg/dL, ALP↑FDG-PET+	Liver, vertebrae, BM	Chemotherapy	Dead (5 months)

the diagnosis. Despite the fact that most EHE patients survive for 5–10 yr after diagnosis, all patients with bone marrow involvement had a poor prognosis, as they were not candidates for surgical resection. Most of the cases with bone marrow involvement died within 16 months from the appearance of symptoms, and had a much more aggressive disease course than other EHE cases; the reported mortality rates are 35% for liver disease and 65% for lung disease (11).

Idiopathic myelofibrosis (IMF) is a hematologic disorder characterized by bone marrow fibrosis. Secondary MF can occur in a wide variety of clinical disorders, such as infections, lymphomas, and some malignancies (12–14). Bone marrow fibrosis in both IMF and MF results in excessive deposits of extracellular matrix (ECM) proteins and the presence of neovascularization (15–17). It has been reported that high levels of fibrogenic cytokines, such as TGF-β and IL-1, are produced by megakaryocytes and monocytes in MF (17–19); the secretion of these cytokines appears to be mediated by interaction between the adhesion molecule of CD44 and ECM proteins (17). Hyaluronan is a high-molecular weight polysaccharide that is present in the ECM of most tissues. Increased serum hyaluronan concentrations have been reported to be associated with tissue damage, inflammatory disease, liver dysfunction, and some malignancies (20–22). Hyaluronan is also known as a potential ligand for the CD44 adhesion molecule. High serum hyaluronan levels have also been reported in MF patients (17, 23).

Histologically, the stroma of EHE varies from being myxomatous to being densely fibrotic. Variable degrees of fibrosis have been noted in most cases of hepatic EHE. Makhlouf *et al.* reported that hyalinization and fibrosis were observed microscopically in 69% of 137 hepatic EHE patients; 62% of these patients had a marked level of fibrosis (4). A similar histopathological pattern has been reported in EHE patients with initial lesions in other organs (2, 8, 24). However, no EHE case with an increased serum hyaluronan level has been reported. In our case, the liver and bone marrow biopsy specimens showed diffuse hyaluronan deposits, and the patient's liver atrophy progressed rapidly over 2 months. High levels of several parameters of fibrogenic mediators, such as hyaluronic acid, TGF-β, and VEGF, were found at the time of diagnosis. The levels of these parameters, especially hyaluronic acid, were markedly increased with the patient's rapid disease progression. These findings suggest that the tumor cells and/or accessory cells secrete hyaluronic acid, and this may reflect this case's severe bone marrow fibrosis.

In conclusion, this is the first case of EHE complicated by severe bone marrow fibrosis. The hyaluronan level increased markedly along with tumor enlargement. Hyaluronan could be used as a marker of EHE activity. In the present case, the hyaluronan level likely played an important role in the pathogenesis of fibrosis. To clarify these points, further investigations of similar cases are needed.

Acknowledgement

We thank Dr K. Shimoda for analyzing the Jak2 mutation.

References

1. Weiss SW, Enzinger FM. Epithelioid hemangioendothelioma: a vascular tumor often mistaken for a carcinoma. *Cancer* 1982;**50**:970–81.
2. Kitaichi M, Nagai S, Nishimura K, Itoh H, Asamoto H, Izumi T, Dail DH. Pulmonary epithelioid haemangioendothelioma in 21 patients, including three with partial spontaneous regression. *Eur Respir J* 1998;**12**:89–96.
3. Lauffer JM, Zimmermann A, Krahenbuhl L, Triller J, Baer HU. Epithelioid hemangioendothelioma of the liver. A rare hepatic tumor. *Cancer* 1996;**78**:2318–27.
4. Makhlouf HR, Ishak KG, Goodman ZD. Epithelioid hemangioendothelioma of the liver: a clinicopathologic study of 137 cases. *Cancer* 1999;**85**:562–82.
5. Suster S, Moran CA, Koss MN. Epithelioid hemangioendothelioma of the anterior mediastinum. Clinicopathologic, immunohistochemical, and ultrastructural analysis of 12 cases. *Am J Surg Pathol* 1994;**18**: 871–81.
6. Díaz R, Sgura Á, Calderero V, Cervera I, Aparicio J, Jordá MV, Pellín L. Central nervous system metastases of pulmonary epithelioid haemangioendothelioma. *Eur Respir J* 2004;**23**:483–6.
7. Kleer CG, Unni KK, McLeod RA. Epithelioid hemangioendothelioma of bone. *Am J Surg Pathol* 1996;**20**:1301–11.
8. Boudousquine AC, Lawce HJ, Sherman R, Olson S, Magenis E, Corless CL. Complex translocation (7; 22) identified in an epithelioid hemangioendothelioma. *Cancer Genet Cytogenet* 1996;**92**:116–21.
9. Leonardou P, Semelka RC, Mastropasqua M, Kanematsu M, Woosley JT. Epithelioid hemangioendothelioma of the liver: MR imaging findings. *Magn Reson Imaging* 2002;**20**:631–3.
10. Cheze-Le Rest C, Botton E, Robinet G, Conan-Charlet V, Bizais Y, Visvikis D. FDG PET in epithelioid hemangioendothelioma. *Clin Nucl Med* 2004;**29**:789–92.
11. Bollinger BK, Laskin WB, Knight CB. Epithelioid hemangioendothelioma with multiple site involvement. Literature review and observations. *Cancer* 1994;**73**:610–5.
12. McCarthy DM. Fibrosis of the bone marrow: content and causes. *Br J Haematol* 1985;**59**:1–7.
13. Hshim MS, Korodofani Ay, el Dabi MA. Tuberculosis and myelofibrosis in children: a report. *Ann Trop Paediatr* 1997;**17**:61–65.

14. Abe Y, Ohshima K, Shiratsuchi M, Honda K, Nishimura J, Nawata H, Muta K. Cytotoxic T-cell lymphoma presenting as secondary myelofibrosis with high levels of PDGF and TGF-β. *Eur J Haematol* 2001;**66**:210–2.
15. Golde DW, Hockking WG, Quan SG, Sparkes RS, Gale RP. Origin of human bone marrow fibrosis. *Br J Haematol* 1980;**44**:183–7.
16. Jacobson RJ, Salo A, Fialkow PJ. Agnogenic myeloid metaplasia: a clonal proliferation of hematopoietic stem cells with secondary myelofibrosis. *Blood* 1978;**51**:189.
17. Rameshwar P, Denny TN, Stein D, Gascon P. Monocyte adhesion in patients with bone marrow fibrosis is required for the production of fibrogenic cytokines. Potential role for interleukin-1 and TGF-b. *J Immunol* 1994;**153**:2819–30.
18. Castro-Malaspina H, Rabellino EM, Yen A, Nachman RL, Moore MAS. Human megakaryocyte stimulation of proliferation of bone marrow fibroblasts. *Blood* 1981;**57**:781–7.
19. Ciurea SO, Merchant D, Mahmud N, Ishii T, Zhao Y, Hu W, Bruno E, Barosi G, Xu M, Hoffman R. Pivotal contributions of megakaryocytes to the biology of idiopathic myelofibrosis. *Blood* 2007; (in press).
20. Rosenberg WMC, Voelker M, Thiel R, Becka M, Burt A, Schuppan D, Hubscher S, Roskams T, Pinzani M, Arthur MJP. Serum markers detect the presence of liver fibrosis: a cohort study. *Gastroenterology* 2004;**127**: 1704–13.
21. West DC, Yqoob M. Serum hyaluronan levels follow disease activity in vasculitis. *Clin Nephrol* 1997;**48**:9–15.
22. Dahl IMS, Turesson I, Holmberg E, Lilja K. Serum hyaluronan in patients with multiple myeloma: correlation with survival and Ig concentration. *Blood* 1999;**93**:4144–8.
23. Hasselbalch H, Junker P, Lisse I, Lindqvist U, Engstrom Laurent A. Circulating hyaluronan in the myelofibrosis/osteomyelosclerosis syndrome and other myeloproliferative disorders. *Am J Hematol* 1991;**36**:1–8.
24. Rosenthal DI, Trear ME, Mankin HJ, Rosenberg AE, Jennings CL. Treatment of epithelioid hemangioendothelioma of bone using a novel combined approach. *Skeletal Radiol* 2001;**30**:219–22.

Inhibition of tumor growth through suppression of angiogenesis by brain-specific angiogenesis inhibitor 1 gene transfer in murine renal cell carcinoma

SHIGETAKA KUDO[1], RYUICHIRO KONDA[1], WATARU OBARA[1], DAISUKE KUDO[1], KENZABURO TANI[2], YUSUKE NAKAMURA[3] and TOMOAKI FUJIOKA[1]

[1]Department of Urology, Iwate Medical University School of Medicine, Morioka; [2]Division of Molecular and Clinical Genetics, Medical Institute of Bioregulation, Kyushu University Hospital, Kyushu University, Fukuoka 812-8582; [3]Laboratory of Molecular Medicine, Human Genome Center, Institute of Medical Science, The University of Tokyo, Tokyo 108-8639, Japan

Received March 17, 2007; Accepted April 26, 2007

Abstract. This study was designed to elucidate the therapeutic effect of transfering the brain-specific angiogenesis inhibitor 1 (BAI1) gene to a mouse renal cell carcinoma cell line (Renca). Female BALB/c mice were inoculated subcutaneously with wild-type Renca (Renca/Wild) cells or Renca cells transfected with the BAI-1 (Renca/BAI-1) or LacZ (Renca/LacZ) gene. Tumor growth was observed every other day from 3 to 35 days after implantation. Moreover, the intratumoral injection of the adenovirus vector containing the gene encoding BAI1 was conducted at two-day intervals from 11 to 31 days after implantation of the Renca/Wild or Renca/BAI1 tumor. Tumor blood flow was measured by colorimetric angiogenesis assay (CAA). The concentration of the vascular endothelial growth factor (VEGF) in the cell culture supernatants was determined by enzyme-linked immunoassay. The size of the Renca/BAI1 tumor was significantly ($p<0.01$) suppressed compared to the Renca/Wild and Renca/LacZ tumors 21 days after tumor implantation. The injection of the BAI1 viral vector at 2-day intervals significantly inhibited the growth of both the Renca/Wild and Renca/BAI1 tumors. The blood volume measured by CAA and microvessel density was significantly lower in the Renca/BAI1 than in the Renca/Wild and Renca/LacZ tumors ($p<0.01$ and $p<0.05$, respectively). A significant ($p<0.01$) reduction in VEGF concentration in the supernatant was demonstrated in the Renca/BAI1 compared with the Renca/Wild and Renca/LacZ cell cultures. These observations suggest that the transfer of the BAI1 gene to Renca can suppress the tumor growth via the inhibition of angiogenesis. The down-regulation of VEGF production in tumor cells contributes to this anti-tumor effect.

Correspondence to: Dr Ryuichiro Konda, Department of Urology, Iwate Medical University School of Medicine, 19-1 Uchimaru, Morioka 020-8505, Japan
E-mail: ryukonda@iwate-med.ac.jp

Abbreviations: BAI1, brain-specific angiogenesis inhibitor 1; RCC, renal cell carcinoma; TSP, thrombospondin; VEGF, vascular endothelial growth factor

Key words: gene therapy, angiogenesis, brain-specific angiogenesis inhibitor 1, renal cell carcinoma

Introduction

New vascular formation is required for tumor growth, invasion and metastasis (1,2). Various factors that regulate angiogenesis have been elucidated successively over the years, and cancer treatments that target these factors have been devised (1,2). Radical nephrectomy or nephron-sparing surgery is the main-stay of curative treatment for localized renal cell carcinoma (RCC), which is unresponsive to radiotherapy and also refractory to chemotherapy (3). Immunotherapies using interferons and interleukin 2 have been used for advanced RCC. However, the two therapies alone as well as in conjunction have demonstrated disappointing success rates of 20% or less (4). RCC is a typical hypervascular tumor, and neovascularisation is thought to play a principal role in tumor progression (5). The inhibition of angiogenesis could lead to promising developments of new treatment modalities.

A brain-specific cancer-regulating p53 target gene was isolated and identified as a new angiogenesis inhibitor, and was named the brain-specific angiogenesis inhibitor 1 (BAI1) gene (6). The BAI1 gene encodes a 1584-amino-acid product containing five thrombospondin (TSP) type 1 repeats. A recombinant protein analogous to the TSP type 1 repeats of this gene product has been shown to inhibit angiogenesis induced by the basic fibroblast growth factor (bFGF) in the rat cornea (6). Although BAI1 mRNA was initially reported to be expressed specifically in the brain, this gene has subsequently been demonstrated in the neoplastic and/or nonneoplastic tissues of the colon, stomach and lung, and its expression correlates inversely with vascular density (7-9).

The overexpression of BAI1 inhibited tumor growth by suppressing tumor angiogenesis in human pancreatic adenocarcinoma cells (Panc-1) (10). Moreover, the overexpression of BAI1 induced cell death in human umbilical vein endothelial cells (10,11).

We designed this study in order to elucidate the possibility of gene therapy by BAI1 gene transfer in RCC. Gene transfer in a mouse RCC cell line (Renca) was conducted using replication-deficient recombinant adenoviral vectors encoding BAI1 (10). Tumor growth was observed after the subcutaneous inoculation of Renca cells transfected with the BAI1 gene and compared with wild-type cells and cells transfected with LacZ. In addition, we evaluated whether the anti-tumor effect of the BAI1 gene transfer is associated with the inhibition of new vascular formation.

Materials and methods

Reagents. A commercial MTT [3-(4,5-dimethylthiazol-2-yl)-2,5-diphenyltetraslium bromide] colorimetry kit was purchased from Chemico (Temecula, CA, USA). X-gal staining solution was from Gibco BRL (Tokyo, Japan) and used at 37°C. An RNeasy Mini Kit was purchased from Qiagen (Tokyo, Japan). The commercial ELISA kits (human bFGF ANALYZA ELISA and mouse VEGF ANALYZA ELISA) were from Genzyme (Minneapolis, USA).

Cell lines and animals. The mouse RCC cell line (Renca) was kindly provided by Dr R.H. Wiltrout (N.C.I., Fredrick, MD), which was maintained *in vivo* by serial intrarenal passage. *In vitro* culture of the Renca cells was performed in RPMI-1640 containing 10% fetal cow serum (FCS) at 37°C under 5% CO_2 (13). Female, euthymic BALB/c mice were housed in a special pathogen-free facility and used routinely at 8 to 10 weeks of age when they weighed 22 to 24 g.

Gene transfection and in vitro tumor growth. Gene transfer in the Renca cells was conducted using the replication-deficient recombinant adenoviral vector encoding the full length cDNA of BAI1 (Renca/BAI1) or LacZ (Renca/LacZ), at a multiplicity of infection (MOI) of 20 for 72 h as described previously (10,12). Renca cells not transfected with any gene (Renca/Wild) were used as the controls.

For the *in vitro* cytotoxicity test, Renca cells ($1x10^5$/well) and the viral vector at an MOI of 1, 2, 10, 20, 50, 100, 200 and 300 were added to a 96-well microplate. After incubation for 72 h, the MTT reagent was added and the cells were incubated for a further 4 h. The reaction was then stopped by the addition of isopropanol hydrochloride, and the absorbance (540 nm) was measured.

In order to confirm the vector transfer efficiency, Renca cells were transfected with the control vector (AdexCA-LacZ) at an MOI of 20 for 72 h and ß-galactosidase was assayed using X-gal staining. The Renca/LacZ cells were fixed in 2% formaldehyde and 0.2% glutaraldehyde in PBS(-) for 10 min at 4°C. The fixative was removed, and then X-gal staining solution was added. After 3 h of reaction at 37°C, the cells were examined under a light microscope.

In order to measure the *in vitro* cellular proliferation capability, Renca cells ($1x10^5$) inoculated in a 25 cm^2 tissue culture flask were transfected with the virus vector (AdexCA-LacZ or pAdex1Cawt-BAI1) at an MOI of 20, and cell counts were performed on days 1, 3, 5 and 7.

Confirmation of the BAI1 gene transfer using RT-PCR. RNA was extracted from Renca/Wild, Renca/LacZ and Renca/BAI1 cells using the RNeasy Mini Kit, and subjected to RT reaction using oligo(dT)12-18 and SuperScript II (Gibco BRL) at 37°C for 90 min. PCR was then performed using Taq Gold DNA polymerase (Applied Biosystems, Tokyo, Japan) and the primers given below. The thermal conditions were 95°C for 10 min, followed by 35 cycles (94°C for 30 sec, 55°C for 30 sec, at 72°C for 60 sec), and a final extension at 72°C for 10 min. The PCR products were electrophoresed on a 1.5% agarose gel, stained with ethidium bromide, and examined under UV light. The primers used were G3PDH, 5'-TGAAGGTCGGTGTGAACGGATTTGGC-3' (sense) and 5'-CATGTAGGCCATGAGGTCCACCAC-3' (anti-sense); BAI1 (6), 5'-ACTCATCCTGCGACGGTGTG-3' (sense, E1S) and 5'-TCCCTCAGGTCCTTCATGCG-3' (anti-sense, E1A). The RT-PCR products obtained in the above manner were fluorescent dyed using the BigDye Terminator (Applied Biosystems), and the base sequences were determined using the ABI PRISM310 Genetic Analyser.

Assay of bFGH and VEGF in cell culture supernatant. Supernatants were obtained from the Renca/Wild, Renca/LacZ and Renca/BAI1 (n=5) cell cultures on days 1, 3, 5 and 7. Concentrations of bFGF and the vascular endothelial growth factor (VEGF) were determined using the commercial ELISA kits mentioned above.

In vivo tumor growth. Renca/Wild, Renca/LacZ or Renca/BAI1 cells ($1x10^6$ cells in 0.05 ml) were inoculated subcutaneously into the dorsal skin of mice (n=10). The tumors were observed on consecutive days for 35 days, and the long and short diameters of the tumors were measured. Tumor volume was estimated according to the following formula, and used as a measure of the antitumor effects: Tumor volume (mm^3) = (short diameter)^2 x (long diameter) x 0.5 (13).

In order to examine the changes in BAI mRNA expression during the experimental period, we obtained Renca/BAI1 tumor tissues on days 3, 5, 9, 15, 21, 29. RNA was extracted from these tissues and subjected to RT-PCR using the same method used for the cultured Renca cells.

Tumor angiogenesis assay. Tumor neovascularisation activity and intratumor blood volume was determined using *in vivo* colorimetric angiogenesis assay (CAA) (13). Renca/Wild, Renca/LacZ or Renca/BAI1 cells ($2x10^6$ cells in 0.05 ml per site) were inoculated subcutaneoulsy into 4 sites of the dorsal skin of a mouse (n=8 per group). After 72 h, 0.25 ml 1% Evan's blue solution was injected into the caudal vein, and the tumors were removed 2 min later. The specimens of these tumors were dissolved in 0.35 ml sodium sulfate/acetone, and the absorbance (620 nm) of the supernatant thus obtained was measured with an ELISA reader. Mouse blood collected after the injection of Evan's blue was dissolved in the same solvent and serially diluted. The blood volume was then calculated using the absorbance of the

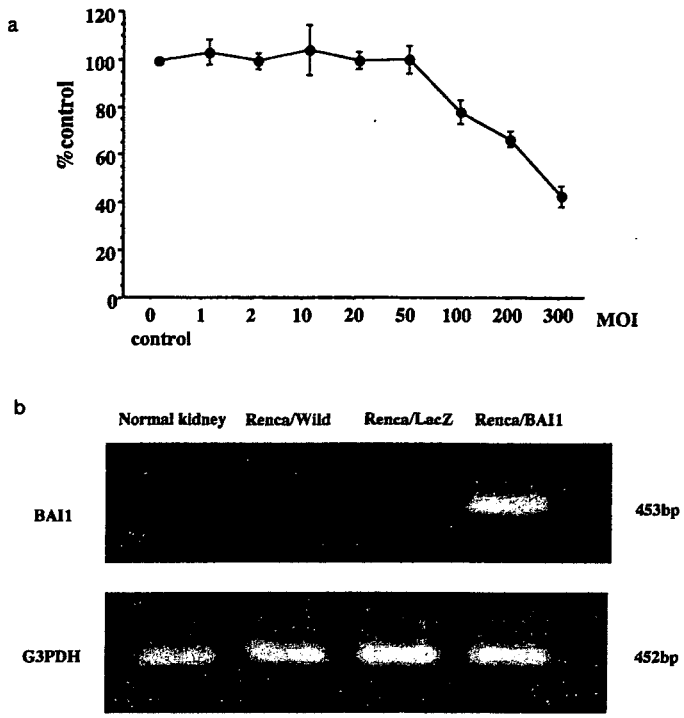

Figure 1. (a) *In vitro* cytotoxic effect of the viral vector at various multiplicities of infection (MOI) on the Renca cell culture. MTT assay was performed in duplicate. No cytotoxicity was observed when virus vectors were added at MOI 50 or less. (b) RT-PCR of the three Renca cell lines and normal kidney tissue. The expression of BAI1 was detected only in the Renca cells transfected with BAI1.

supernatant obtained from serially diluted mouse blood samples as the standard. The total blood volume of 2 transplant sites was defined as the tumor neovascularisation activity. Normal samples were obtained from non-inoculated sites in order to measure the blood volume in the non-tumor regions.

Immunohistochemistry and quantification of microvessel density. Immunostaining for CD31 was performed on 3-5 μm sections from paraffin-embedded tumor tissues (n=6) on day 15 using rat anti-mouse CD31 (BD Pharmingen, San Diego, USA).

Intratumoral microvessel density (MVD) was determined by light microscopy after immunostaining the sections with anti-CD31 antibody. The MVD was expressed as the average number of the 5 highest areas identified within a single x200 per fields.

Intratumor administration of BAI1 gene vector. Twenty microliters of pAdex1Cawt-BAI1 ($1.7x10^8$ pfu/ml) or PBS(-) were injected into the subcutaneously implanted Renca/Wild or Renca/BAI1 tumor, starting on the 11th day after implantation and continuing on every other day for a total of 11 doses (n=10 for each group). Tumor volume was estimated using the same formula as described above.

Statistical analysis. The Mann-Whitney U test was used for the statistical analysis of the comparative data. Values of $p<0.05$ were considered significant.

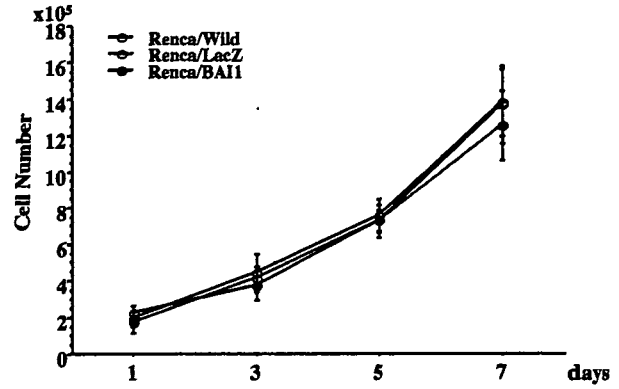

Figure 2. *In vitro* proliferation capability of Renca/Wild, Renca/LacZ and Renca/BAI1 cells. No significant difference was observed among the three cell lines.

Results

In vitro tumor growth. No cytotoxicity was observed by the addition of the virus vectors at MOI 50 or less, but toxicity was seen at MOI 100 or higher (Fig. 1a). Therefore, subsequent viral vector transfection experiments were performed using an MOI of 20 in order to eliminate the possibility of vector cytotoxicity. Beta-galactosidase staining of the Lac Z transfectants (MOI 20) confirmed a very high infection rate (almost 100%) of tumor cells by adenovirus-mediated transfer. The results of RT-PCR of the RNA samples obtained from normal mouse kidney tissues (n=3) and the three Renca cell lines are shown in Fig. 1b. A strong 453 bp band was seen only in the RNA sample of Renca/BAI1 cells, signifying that the BAI1 gene was transferred to the Renca cells. The base sequence for the PCR products obtained from the Renca/BAI1 cells exactly matched that for the human BAI1 gene (6).

Fig. 2 shows the *in vitro* proliferation capability of the Renca/Wild, Renca/LacZ and Renca/BAI1 cells. The cell counts increased ~7-fold in all three cell cultures by the 7th day. No significant difference in the proliferation rate was found among the Renca/Wild, Renca/LacZ and Renca/BAI1 cells.

Concentrations of bFGF and VEGF in cell culture supernatant. Assays of angiogenic factors in the cell culture supernatant are shown in Fig. 3 (n=5 for each group). VEGF levels on days 3, 5 and 7 post-infection with the viral vector were significantly ($p<0.01$) lower in the Renca/BAI1 cells than in the Renca/Wild or Renca/LacZ cells (Fig. 3a). In contrast, no significant differences in the bFGF level were observed among the three cell lines throughout the experimental period (Fig. 3b).

In vivo tumor growth and angiogenesis. Renca/Wild and Renca/LacZ tumors demonstrated rapid growth, as shown by the tumor volume measured up to day 35 (Fig. 4a). In contrast, the growth of the Renca/BAI1 tumor was significantly ($p<0.01$) suppressed from days 27 to 35 compared with the Renca/Wild or Renca/LacZ tumor. The expression of BAI1 mRNA was maintained in the Renca/BAI1 tumors until day 15. However, the attenuation of BAI1 mRNA expression was observed on days 21 and 29 (Fig. 4b).

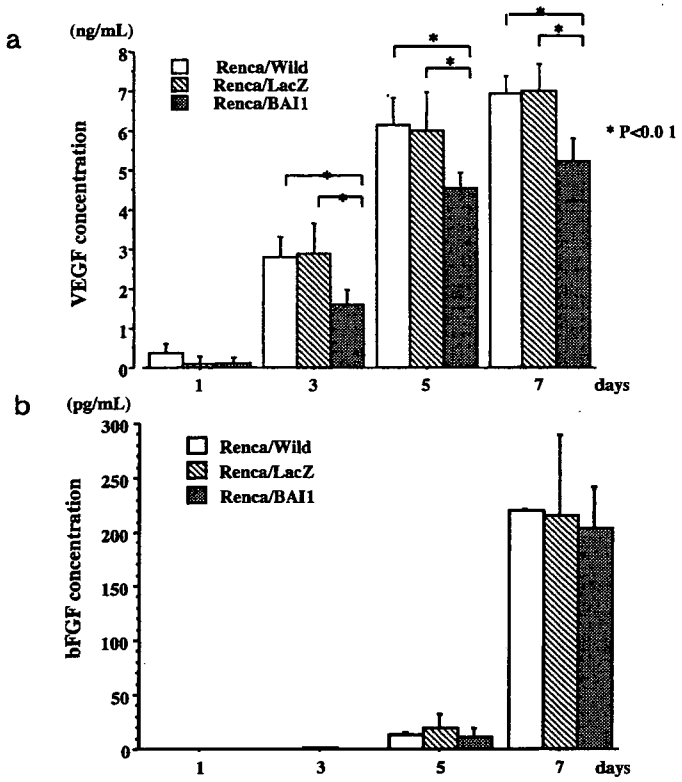

Figure 3. Concentrations of VEGF (a) and bFGF (b) in the cell culture supernatants. The levels of VEGF were significantly lower in the Renca/BAI1 cell culture than in the Renca/Wild and Renca/LacZ cell cultures on days 3, 5 and 7 post-infection (a). No significant differences in the level of bFGF were noted among the three cell cultures (b).

Intratumor blood volumes as measured by the CAA method are shown in Fig. 5a. The blood content (mean ± standard deviation; in μl/66.4 mm^2) of tumors inoculated into the mouse dorsal skin was 10.02±2.97, 10.87±3.06 and 5.44±2.48 in Renca/Wild, Renca/LacZ and Renca/BAI1 tumors, respectively (Fig. 5b). The intratumoral blood volume was significantly ($p<0.01$) lower in the Renca/BAI1 tumor compared with the Renca/Wild or Renca/LacZ tumor. The blood content of normal skin was 1.75±0.88.

Microvessels stained with CD31 were attenuated in the Renca/BAI1 tumors compared with the Renca/Wild and Renca/LacZ tumors (Fig. 6a). MVD was significantly lower in the Renca/BAI1 than in the Renca/Wild and Renca/LacZ tumors ($p<0.05$) (Fig. 6b).

Intratumor BAI1 viral vector injection. Tumor growth was inhibited significantly in the Renca/Wild tumors injected with the BAI1 viral vector compared with the tumors injected with PBS(-) from days 21 to 31 ($p=0.004$ on day 31) (Fig. 7). In addition, the same antitumor effect was found in the Renca/BAI1 tumor injected with the BAI1 viral vector compared with the tumors injected with PBS(-) from days 25 to 31 ($p=0.003$ on day 31) (Fig. 7).

Discussion

Tumor growth and metastasis depend on angiogenesis, and the suppression of new vascular formation is one of the pivotal strategies for inhibiting tumor progression (1,2). A variety of pro- and anti-angiogenic molecules regulates new vascular formation. Angiogenesis is switched off when the effect of pro-angiogenic molecules is balanced by that of anti-angiogenic molecules. In contrast, a net balance tipped in favor of angiogenesis begins the angiogenesis process. Tumors themselves produce some angiogenesis activators and stimulate new vascular formation. Blocking angiogenesis could be an efficacious therapy for preventing tumor growth (1,2). VEGF is one of the principal members of pro-angi-

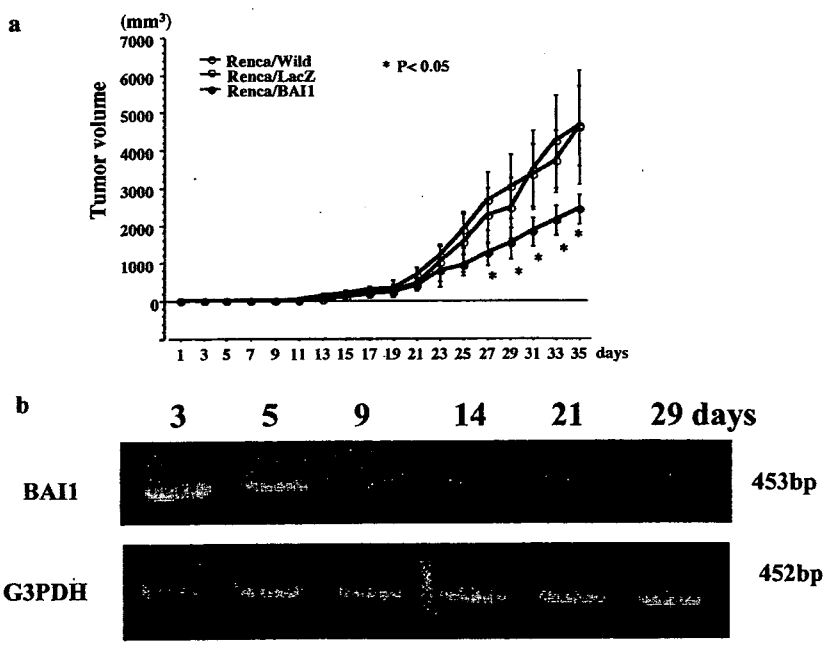

Figure 4. *In vivo* tumor growth up to day 35 after the subcutaneous inoculation of tumor cells (a) and changes in BAI1 mRNA expression in the Renca/BAI1 tumors during the experimental period (b). The volume of the Renca/BAI1 tumor was significantly reduced compared with the Renca/Wild and Renca/LacZ tumors from day 27 onward ($p<0.05$). The expression of BAI1 mRNA was maintained until day 15 (b). On days 21 and 29, BAI1 mRNA expression was attenuated.

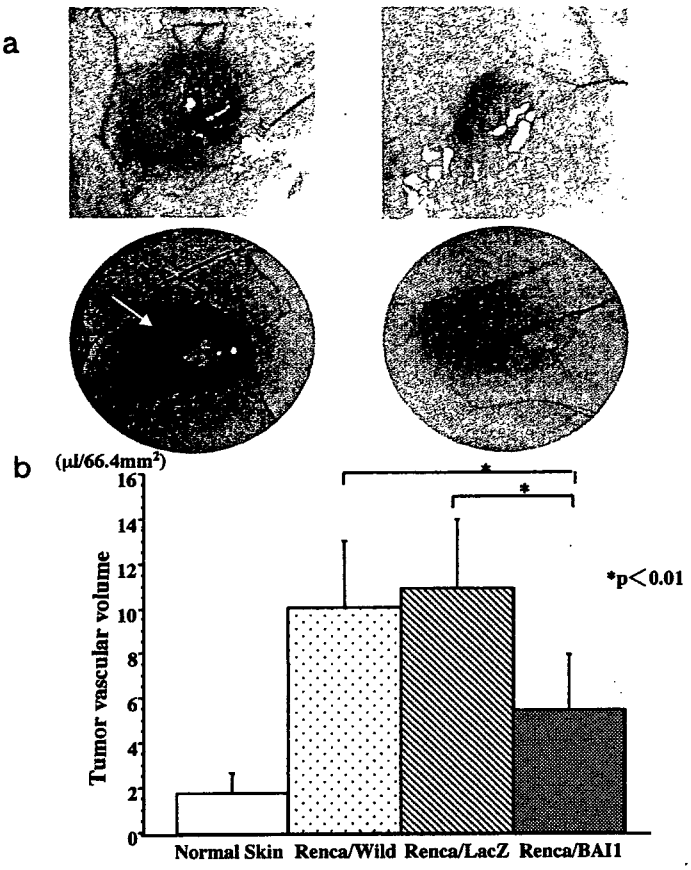

Figure 5. Tumor neovascularisation. (a) Macroscopic findings of tumor vascularization 72 h after subcutaneous inoculation. Angiogenesis is not promoted by Renca/BAI1 cells. In contrast, a stable vascular network is established by Renca/LacZ (arrow). (b) Intra-tumor blood volumes determined by the colorimetric angiogenesis assay method. A significantly lower blood volume was observed in the Renca/BAI1 tumor compared with the Renca/Wild and Renca/LacZ tumors ($p<0.01$).

ogenic molecules and the effectiveness of anti-VEGF therapy in inhibiting tumor growth has been reported (2). On the contrary, BAI that was originally isolated as a p53-target gene possessing an extracellular domain containing TSP type 1 repeats has been considered an inhibitor of angiogenesis (6). *In vivo* experiments have revealed that the transfection of the BAI1 gene into human pancreatic adenocarcinoma cells (Panc-1) results in suppressed tumor growth by inhibiting angiogenesis (10). *In vitro* studies have detected no difference in tumor growth between parental Panc-1 cells and BAI1 or LacZ transfectants, although an antiproliferative effect was found in human umbilical vein endothelial cells after the transfection of the BAI gene. In our *in vivo* study, the Renca/BAI1 tumor implanted subcutaneously into female BAL/c mice demonstrated significantly suppressed growth, while similarly implanted Renca/Wild and Renca/LacZ tumors proliferated rapidly. Intratumor blood volume and MVD were significantly reduced in the Renca/BAI1 tumors compared with the Renca/Wild and Renca/LacZ tumors. Our *in vitro* study showed no difference in cell growth between Renca/BAI1 and Renca/LacZ, consistent with the observation in human pancreatic adenocarcinoma cells (10). Since the BAI1 gene was expressed only in Renca/BAI1 cells and not in Renca/Wild or Renca/LacZ cells on RT-PCR, the suppression of tumor growth in Renca/BAI1 could be attributed to the reduction in vascular formation as a consequence of the BAI1 overexpression.

A peptide containing TSP type 1 repeats suppresses bFGF-induced neovascular formation (6). BAI-1 is a transmembrane protein and has five TSP type 1 repeats and an integrin binding site (RGD motif) in its extracellular domain (6). BAI-1 is proteolytically cleaved at a conserved G-protein-coupled receptor proteolytic cleavage site (GPS), releasing its 120 kDa extracellular domain (14). This extracellular fragment has a potent anti-angiogenic action (11,14). The definite mechanism for the anti-angiogenic effect of BAI1 is being studied, but recent study has reported that the secret extracellular domain of BAI1 exerts anti-proliferative action on the surrounding endothelial cells by blocking αvß5 integrin partly through activating the caspase (11). In a previous *in vitro* study, a reduction in VEGF and matrix metalloproteinase-1 (MMP-1) expression has been demonstrated in a human pancreatic adenocarcinoma cell line (Panc-1) after BAI1, but not after LacZ transfer (10). The present study also showed a reduction in VEGF concentration in the supernatant of the Renca/BAI1 but not the Renca/LacZ cell culture. From these observations, BAI1 shows anti-angiogenic activity not through a direct action on endothelial cells but through indirect effects by inhibiting other factors such as VEGF and MMP-1.

The expression of the BAI1 gene was initially considered to be specific to brain tissue (6). A lack of this gene is thought to be the cause of chaotic vascular proliferation in glioblastoma. However, BAI1 gene expression has subsequently been demonstrated in lung, gastric and colorectal cancer, suggesting that BAI1 plays an important role in the inhibition of angiogenesis associated with a variety of neoplasia other than cerebral tumors (7-9). A significantly lower MVD was demonstrated in lung cancers expressing BAI1 mRNA compared with those not expressing this mRNA (9). In colorectal cancers, the expression of BAI1 mRNA was significantly lower in malignant than in non-malignant colorectal tissues (7). BAI1 gene expression was inversely related to vascular invasion as well as metastasis, and also inversely correlated with vascular density. These two studies suggest that the expression of BAI1 can inhibit new vascular formation and/or tumor metastasis in lung and colorectal cancers. The expression of BAI1 mRNA was also reduced in gastric cancer (8). A significant prolonged survival period after gastrectomy has been demonstrated in patients with good BAI1 expression in the adjacent normal mucosa compared with those with poor BAI1 expression.

In the present study, the transferring of the BAI1 gene to mouse RCC Renca cells via an adenovirus vector resulted in inhibited tumor growth and suppressed tumor angiogenic activity *in vivo*, although tumor cell growth was not inhibited *in vitro*. Transfection of the human pancreatic adenocarcinoma cell line Panc-1 with the BAI gene also resulted in suppressed tumor growth *in vivo* but had no effect on *in vitro* cell growth (10). The inhibition of *in vivo* growth of the BAI-transfected Panc-1 tumor was associated with the suppression of angiogenesis, as was also observed in the BAI1-transferred Renca tumors in the present study. As mentioned above, BAI1 could be one of the principal factors in the suppression

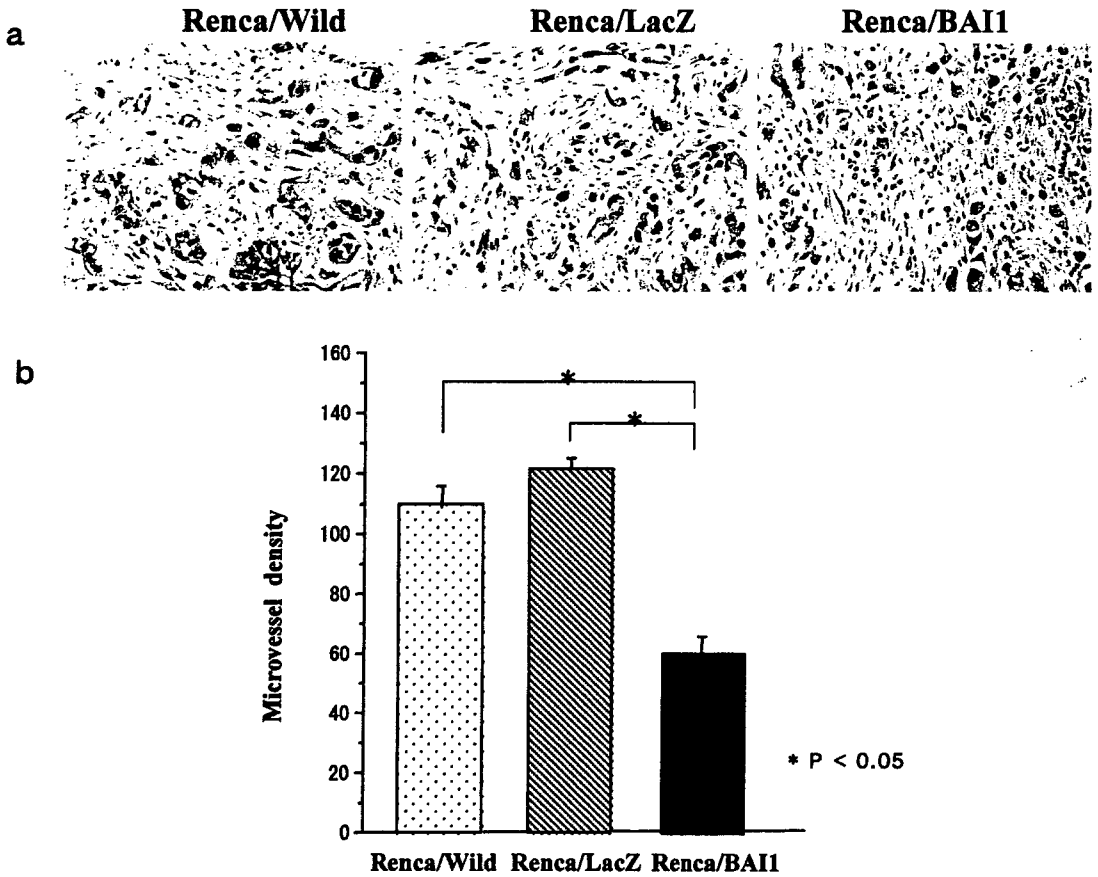

Figure 6. Immunostaining for CD31 (a) and microvessel density (MVD) (b) in Renca/Wild, Renca/LacZ and Renca/BAI1 tumors. The number of microvessels stained with CD31 was lower in the Renca/BAI1 than in the Renca/Wild and Renca/LacZ tumors (a). MVD was significantly lower in the Renca/BAI1 than in the Renca/Wild and Renca/LacZ tumors ($p<0.05$).

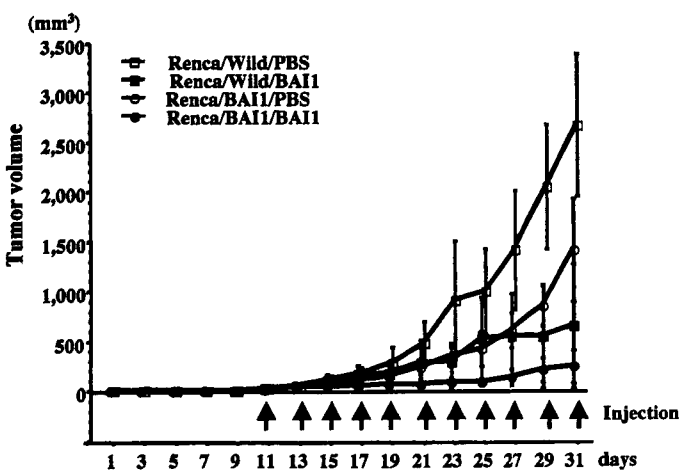

Figure 7. *In vivo* tumor growth after intratumoral injection of the BAI1 viral vector. Repeated BAI1 viral vector injection significantly suppresses tumor growth not only in the Renca/wild tumor but also in the Renca/BAI1 tumor, compared with the PBS(-) injection.

of tumor growth via the inhibition of angiogenesis and should be considered for gene therapy.

In order to examine the possibility of BAI1 as a candidate for gene therapy in RCC, we injected the BAI1 gene vector into subcutaneously implanted Renca/Wild and Renca/BAI1 tumors from the 11th day after implantation at 2-day intervals. The intratumor injection of the BAI1 gene vector significantly inhibited the growth of the Renca/Wild tumor compared with the PBS injection instead of the BAI1 gene. In addition, a significant reduction in the subcutaneously implanted Renca/BAI1 tumor was also achieved by the intratumor injection of the BAI1 gene, in comparison with the PBS injection. These observations could indicate the possibility of BAI gene therapy or the development of efficient drugs based on the extracellular fragment of BAI1 not only for RCC with decreased BAI1 expression but also for those with good BAI1 expression.

We investigated the antitumor effects of the BAI1 gene transfer into the murine RCC cell line, Renca, using replication-deficient recombinant adenovirus vectors encoding the full-length cDNA of BAI1. Significant suppression of both tumor growth and vascular formation was demonstrated in the Renca/BAI1 tumor compared with the Renca/Wild and Renca/LacZ tumors. The concentrations of VEGF were lower in the supernatant of the Renca/BAI1 cell culture compared with the Renca/Wild and Renca/LacZ cell cultures, suggesting that the suppression of VEGF production is involved in the anti-angiogenic effect of BAI1. Growth was inhibited in both the Renca/Wild and Renca/BAI1 tumors upon tumoral injection of a viral vector encoding BAI1, suggesting the possibility of the clinical application of this gene therapy.

Acknowledgements

We deeply thank Professor Izumi Saito (Human Genomic Center, Institute of Medical Science, University of Tokyo) for AdexCA-LacZ, the viral vector containing the LacZ.

References

1. Calmelite P and Rakesh KJ: Angiogenesis in cancer and other disease. Nature 407: 249-257, 2000.
2. Yancopoulos GD, Davis S, Gale NW, *et al*: Vascular-specific growth factors and blood vessel formation. Nature 407: 242-248, 2000.
3. Todd RF III, Garnic MB, George PC, *et al*: Phase I-II trial of methylglyoxal-bis guanylhydrazone (methyl-G) in the treatment of patients with metastatic renal adenocarcinoma. Cancer Treat Res 65: 17-20, 1981.
4. De Kernion JB, Sarna G, Figlin R, *et al*: The treatment of renal cell carcinoma with human leukocyte α-interferon. J Urol 130: 1063-1066, 1983.
5. Campbell SC: Advances in angiogenesis res earch. Relevance to urological oncology. J Urol 158: 1663-1674, 1997.
6. Nishimori H, Shiratsuti T, Urano T, *et al*: A novel brain-specific p53-target gene, BAI1, containing thrombospondin type 1 repeats inhibits experimental angiogenesis. Oncogene 15: 2145-2150, 1997.
7. Fukusima Y, Oshika Y, Tsuchida T, *et al*: Brain-specific angiogenesis inhibitor 1 expression is inversely correlated with vascularity and distant metastasis of colorectal cancer. Int J Oncol 13: 967-970, 1998.
8. Heelee JI, Koh JT, Shin BA, *et al*: Comparative study of angiostatic and anti-invasive gene expression as prognostic factors in gastric cancer. Int J Oncol 18: 355-361, 2001.
9. Hatanaka H, Oshika Y, Abe Y, *et al*: Vascularization is decreased in pulmonary adenocarcinoma expressing brain-specific angiogenesis inhibitor1 (BAI1). Int J Mol Med 5: 181-183, 2000.
10. Duda DG, Sunamura M, Lozonschi L, *et al*: Overexpression of the p53-inducible brain-specific angiogenesis inhibitor 1 suppresses efficiently tumour angiogenesis. Br J Cancer 86: 490-496, 2002.
11. Koh JT, Kook H, Kee HJ, *et al*: Extracellular fragment of brain-specific angiogenesis inhibitor 1 suppresses endothelial cell proliferation by blocking αvß5 integrin. Exp Cell Res 294: 172-184, 2004.
12. Nishizaki M, Fujiwara T, Tanida T, *et al*: Recombinant adenovirus expressing wild-type p53 is antiangiogenic: A proposed mechanism for bystander effect. Clin Cancer Res 5: 1015-1023,1999.
13. Fujioka T, Hasegawa M, Ogiu K, *et al*: Antitumor effects of angiogenesis inhibitor 0-(chloroacetyl-carbamoyl) fumagillol (TNP-470) agents in murin renal cell carcinoma. J Urol 155: 1775-1778, 1996.
14. Kaur B, Brat DJ, Devi NS, *et al*: Vasculostatin, a proteolytic fragment of brain angiogenesis inhibitor 1, is an antiangiogenic and antitumorigenic factor. Oncogene 24: 3632-3642, 2005.

and managed him as an outpatient for the following 18 months.

Comment

Considering all factors, such as the temporal relationship between the seizure onset and quetiapine intake, the exclusion of other possible etiology of seizures and their cessation after drug withdrawal, we judged that quetiapine precipitated seizure activity in both patients. These cases serve as a reminder that postmarketing surveillance of newly released medications, clinical awareness of seizure potential when using these medications, and the need for risk factor evaluation before starting psychotropic medications are essential.

IREM YALUG, M.D.
Department of Psychiatry, Kocaeli University, Kocaeli, Turkey
ALI EVREN TUFAN, M.D.
Department of Child and Adolescent Psychiatry, Kocaeli University, Kocaeli, Turkey
LEVENT KAYAALP, M.D.
Department of Child and Adolescent Psychiatry, Istanbul University, Kocaeli, Turkey

References

1. Aman MG, Lindsay RL, Nash PL, et al: Individuals with mental retardation, in Pediatric Psychopharmacology Principles and Practice. Edited by Martin A, Scahill L, Charney DS, et al. New York, Oxford University Press, 2003, pp 617–630
2. Cummings MR, Miller BD: Pharmacologic management of behavioral instability in medically ill pediatric patients. Curr Opin Pediatr 2004; 16:516–522

Familial Turner Mosaicism 46XX/45XO With Brain Calcification

SIR: A 72-year-old woman presented with mild diabetes mellitus, brain calcification with no obvious neurological deficit, and mosaic 45XO/46XX. Her daughter presented with mosaic 45XO/46XX Turner syndrome with deafness, facial involuntary movement, primary amenorrhea, and marked brain calcification with mild hypoparathyroidism.[1]

Her mother had experienced normal menarche, menstral cycle, and birth. The mother's serum calcium, phosphorus, and parathyroid hormone levels were within normal limits. The ratio of 46XX and 45XO was 85%:15% (40 cells examined) in the daughter and 75%:25% (20 cells examined) in the mother. Her symptoms were much milder than the daughter's, implying that their genetic defect yielded genetic anticipation. There had been some familial cases of brain calcinosis, known as Fahr disease, in which genetic anticipation had been often observed (i.e., descendent generation reveals severer phenotype). Recently, a locus around a tuberin-like protein gene 1 (*TULIP1*) at 14q.13-q21.1 was proposed as a candidate locus for Fahr disease.[2] Genetic anticipation has been observed in association with nucleotide repeat expansion,[3] and we searched the 14q.13-q21.1 region for nucleotide repeats through the NCBI BLAST Search (i.e., 10 kinds of trinucleotide-repeat, AAC, AAG, AAT, ACC, ACG, ACT, AGG, ATC, CAG, and CCG), and tetra-nucleotide CCTG[4] and penta-nucleotide repeat ATTCT,[5] which have been reported to cause diseases with genetic anticipation when they expand in certain genes. We identified 36 loci, including the nucleotide repeat in 14q.13-q21.1, but failed to detect any significant expansion of the analyzed nucleotide repeats in the patient and the patient's daughter.

Turner syndrome is characterized by impaired physical growth and hypogonadism. But some rare cases with 45XO or mosaicism of 45XO/46XX were reported to bear children, some of whom revealed chromosomal abnormality including mosaicism, implying that a genetic defect predisposing to chromosomal fragility yielding chromosomal aneuploidy was hereditarily transmitted to the descendents in those familial cases.[6,7] A few reported cases of Turner syndrome accompanied by brain calcification.[1] Some chromosomal instability syndromes with impaired DNA repair mechanisms, such as Cochayne syndrome and Fanconi anemia, which often reveal chromosomal aneuploidy,[8] accompany brain calcification.[9,10] The combination of chromosomal aneuploidy and brain calcification may be caused by a genetic defect concerning chromosomal instability.

The candidate locus for familial Fahr disease is proposed to locate around *TULIP1* at chromosome 14q.13-q21.1, but the *TULIP1* gene contains no nucleotide repeat. Impaired *TULIP1* function may be associated with structural alteration of unknown genes containing nucleotide repeats, or cause the genetic anticipation by an unknown mechanism. The genetic anticipation with Fahr disease may be yielded by an unknown mechanism other than nucleotide repeat expansion, or by nucleotide-repeat expansion coming out of 14q.13-q21.1, or by expansion of unknown nucleotide repeat other than analyzed here (i.e., dinucleotide or hexanucleotide repeat).

TOYOKI MAEDA, M.D., PH.D.
MASAHIRO SUGANO, M.D., PH.D.
JING-ZHI GUAN, M.D., PH.D.
JUN-ICHI OYAMA, MD. PH.D.
YOSHIHIRO HIGUCHI, M.D., PH.D.
NAOKI MAKINO, M.D., PH.D.
Division of Molecular and Clinical Gerontology, Department of Molecular and Cellular

Biology, Medical Institute of Bioregulation, Oita, Japan
MASAMITSU HATAKENAKA, M.D., PH.D
Department of Clinical Radiology, Graduate School of Medical Sciences, Kyushu University, Fukuoke, Japan
HIROMI MUTA, M.D., PH.D.
MASAHARU NAKAYAMA, M.D., PH.D.
YUKOH NAKAZAKI, PH.D.
RYO KURITA, PH.D.
TAKASHI HIROYAMA, PH.D.
TOMOKAZU SUZUKI, M.D. PH.D.
KENZABURO TANI, M.D., PH.D.
Division of Molecular and Clinical Genetics, Department of Molecular Genetics, Medical Institute of Bioregulation, Kyushu University, Fukuoka, Japan

This work was supported, in part, by a Grant-in-Aid from the Ministry of Education, Science, and Culture of Japan.

References

1. Suzuki Y, Watanabe H, Haeno S, et al: Primary hypoparathyroidism in Turner's syndrome. Intern Med 1995; 34:1071–1073
2. Schwarzbraun T, Vincent JB, Schumacher A, et al: Cloning, genomic structure, and expression profiles of tulip1 (GARNL1), a brain-expressed candidate gene for 14q13-linked neurological phenotypes, and its murine homologue. Genomics 2004; 84:577–586
3. Lindblad K, Schalling M: Expanded repeat sequences and disease. Seminars in Neurol 1999; 19:289–299
4. Matsuura T, Yamagata T, Burgess DL, et al: Large expansion of the attct pentanucleotide repeat in spinocerebellar ataxia type 10. Nat Genet 2000; 26:191–194
5. Liquori CL, Ricker K, Moseley ML, et al: Myotonic dystrophy type 2 caused by a cctg expansion in intron 1 of ZNF9. Science 2001; 293:864–867
6. Ayuso MC, Bello MJ, Benitez J, et al: Two fertile turner women in a family. Clin Genet 1984; 26:591–596
7. Birkebaek NH, Cruger D, Hansen J, et al: Fertility and pregnancy outcome in danish women with turner syndrome. Clin Genet 2002; 61:35–39
8. Callen E, Ramirez MJ, Creus A, et al: Relationship between chromosome fragility, aneuploidy and severity of the haematological disease in fanconi anaemia. Mut Res 2002; 504:75–83
9. Gayatri NA, Hughes MI, Lloyd IC, et al: Association of the congenital bone marrow failure syndromes with retinopathy, intracerebral calcification and progressive neurological impairment. Eur J Paediat Neurol 2002; 6:125–128
10. Demaerel P, Kendall BE, Kingsley D: Cranial CT and MRI in diseases with DNA repair defects. Neuroradiology 1992; 34:117–121

Exploring the Relationship Between Panic Disorder and Parkinson's Disease

SIR: I read with interest the recent report by Matsui et al.[1] in which the authors highlighted a patient who was diagnosed with Parkinson's disease shortly after a panic attack. Though there is strong biological basis for the association of panic disorder with Parkinson's disease, the case report raises a number of unanswered questions. Based on the presentation, one cannot exclude the possibility of chance occurrence of the two conditions. The onset of parkinsonian symptoms in their patient may be much earlier than the date when the patient first noticed them. It may be more convincing if longitudinal data were available where it can be shown that the two problems progressed in tandem. Furthermore, availability of detailed information on the patient's premorbid personality and family history of psychiatric disorder would have been useful.

I think the more interesting clinical question would be to determine the proportion of Parkinson's disease patients who present with panic disorder before or at the time of diagnosis. To address that, I interviewed and examined 53 consecutive newly diagnosed Parkinson's disease patients in our movement disorders clinic for evidence and history of panic disorder prior to the diagnosis. This was carried out as part of our routine clinical care, and I also received institutional ethics approval for evaluation of nonmotor symptoms in Parkinson's disease. The patients' mean age of onset was 62 (SD = 11.5) years, with about 50% men and with the Hoehn and Yahr stage between 1 to 4. I found that none of our patients had history or evidence of panic disorder prior to Parkinson's disease diagnosis. This suggests that panic disorder as a presentation prior to the onset of Parkinson's disease symptoms was uncommon, at least in our population. Whether our finding reflects ethnicity-specific effects of phenotypic expression remains to be clarified.

However, I agree that psychiatric nonmotor symptoms, such as anxiety, depression, and panic disorder, can be disabling in Parkinson's disease patients,[2,3] and these are relatively less well studied than motor disability. Among anxiety disorders, it appears that generalized anxiety disorder, panic disorder and social phobias are most frequently encountered, and anxiety may develop before motor features.[3] To further our understanding of the pathophysiology of panic disorder in Parkinson's disease, more prospective studies are needed to examine their cause-effect relationship and the temporal relationship of panic disorder with other psychiatric and cognitive disturbances.

ENG-KING TAN, M.D., M.R.C.P.
Department of Neurology, Singapore General Hospital, National Neuroscience Institute, Singapore

References

1. Matsui H, Udaka F, Oda M, et al: Parkinson's disease following panic disor-

GASTROENTEROLOGY 2008;134:447–458

BASIC–ALIMENTARY TRACT

A Critical Role of CD30 Ligand/CD30 in Controlling Inflammatory Bowel Diseases in Mice

XUN SUN,* SHINICHI SOMADA,‡ KENSUKE SHIBATA,* HIROMI MUTA,‡ HISAKATA YAMADA,* HIROFUMI YOSHIHARA,* KUNIOMI HONDA,§ KAZUHIKO NAKAMURA,§ RYHOICHI TAKAYANAGI,§ KENZABURO TANI,‡ ECKHARD R. PODACK,† and YASUNOBU YOSHIKAI*

*Division of Host Defense and ‡Division of Molecular Genetics, Medical Institute of Bioregulation, and §Department of Medicine and Bioregulatory Science, Kyushu University, Fukuoka, Japan; and †Department of Microbiology and Immunology, University of Miami, Miami, Florida

Background & Aims: **A CD30-ligand (CD30L) is a 40-kilodalton, type II membrane-associated glycoprotein belonging to the tumor necrosis factor family. Serum levels of soluble CD30 increased in inflammatory bowel diseases (IBD), suggesting that CD30L/CD30 signaling is involved in the pathogenesis of IBD. In this study, we investigated the role of CD30L in oxazolone (OXA)- and trinitrobenzene sulfonic acid (TNBS)-induced colitis in CD30L knockout (KO) mice.** ***Methods:*** **Colitis was induced by OXA or TNBS in CD30LKO mice with BALB/c or C57BL/6 background, respectively, and diverse clinical signs of the disease were evaluated. Cytokine production from lamina propria T cells of the colon was assessed by enzyme-linked immunosorbent assay. Anti-interleukin (IL)-4 monoclonal antibody (mAb) or agonistic anti-CD30 mAb was inoculated in mice with colitis induced by OXA or TNBS.** ***Results:*** **CD30LKO mice were susceptible to OXA-induced colitis but resistant to TNBS-induced acute colitis. The levels of T helper cell 2 type cytokines such as IL-4 and IL-13 in the LP T cells were significantly higher, but the levels of interferon γ were lower in OXA- or TNBS-treated CD30LKO mice than in wild-type mice. In vivo administration of agonistic anti-CD30 mAb ameliorated OXA-induced colitis but aggravated TNBS-induced colitis in CD30LKO mice.** ***Conclusions:*** **These results suggest that CD30L/CD30 signaling is involved in development of both OXA- and TNBS-induced colitis. Modulation of CD30L/CD30 signaling by mAb could be a novel biologic therapy for IBD.**

Human inflammatory bowel diseases (IBD), including Crohn's disease (CD) and ulcerative colitis (UC), are characterized by inflammation in the large and/or small intestine associated with uncontrolled innate and adaptive immunity against normal constituents, including commensal bacteria and various microbial products.[1–4] The responding T cells exhibit a T helper cell (Th) 1 phenotype capable of producing interferon (IFN)-γ in CD, whereas Th2 cytokines are closely associated with UC.[5–7] Among various experimentally induced colitis models in mice, spontaneous colitis in interleukin (IL)-10-deficient mice,[8] colitis in recombination-activating gene (RAG)-deficient mice transferred with $CD4^+CD45RB^{high}$ T cells,[9] and hapten-induced colitis in mice caused by intrarectal administration of trinitrobenzene sulfonic acid (TNBS)[10–13] are thought of as a Th1-type colitis animal model resembling CD. On the other hand, spontaneous colitis in IL-2-deficient mice[14] or in T-cell receptor (TCR) α-deficient mice[15] resembles UC with Th2-like responses. Another hapten-induced colitis caused by intrarectal administration of oxazolone (OXA) is characterized by inflammation with increased Th2-type cytokine secretion and is thought to be associated with Th2-like responses mediated by $CD4^+$ T cells including natural killer (NK) T cells.[16,17]

A CD30 ligand (CD30L, CD153) is a 40-kilodalton, type II membrane-associated glycoprotein belonging to the tumor necrosis factor (TNF) family[18] and is expressed on both $CD4^+$ Th1 and Th2 cells, although there are several lines of evidence for expression on macrophages, dendritic cells (DC), and B cells.[19–22] CD30, a receptor for CD30L, is expressed preferentially by activated or memory Th2 cells but not by resting B or T cells.[23–26] There are several lines of evidence showing that the CD30L/CD30 signaling is involved in Th2 cell responses and Th2-associated diseases.[23–26] However, a number of recent studies suggested that CD30L/CD30 signaling is also linked to Th1 cell responses and Th1-associated diseases.[27–30] Serum levels of soluble CD30 (sCD30) increased in UC, suggesting that CD30L/CD30 signaling is involved in the pathogenesis of IBD.[31] However, little is known about the roles of CD30L/CD30 signaling in IBD.

In the present study, to verify the roles of CD30L in IBD, we examined susceptibility of CD30L knockout

Abbreviations used in this paper: Ag, antigen; APC, allophycocyanin; CD, Crohn's disease; CD30L, CD30 ligand; DC, dendritic cell; KO, knockout; LPL, lamina propria lympocyte; mAb, monoclonal antibody; OXA, oxazolone; TNBS, trinitrobenzene sulfonic acid; UC, ulcerative colitis.

0016-5085/08/$34.00
doi:10.1053/j.gastro.2007.11.004

(KO) to OXA- or TNBS-induced colitis, 2 representative colitis models for IBD. CD30LKO mice were highly susceptibile to OXA-induced colitis but resistant to TNBS-induced acute colitis. In vivo administration of agonistic anti-CD30 monoclonal antibody (mAb) ameliorated OXA-induced colitis but aggravated TNBS-induced acute colitis in CD30LKO mice. These results suggest that CD30L is involved in development of both types of IBD. Implications of these findings for a novel biologic therapy in controlling IBD are discussed.

Materials and Methods

Mice

Age- and sex-matched BALB/c or C57BL/6 male mice were obtained from Charles River Laboratories (Atsugi, Japan). The generation of CD30LKO mice with BALB/c background were described previously.[32,33] CD30LKO mice with C57BL/6 background were backcrossed into C57BL/6 mice more than 8 times, and their littermates were used as control. This study was approved by the Committee of Ethics on Animal Experiment in Faculty of Medicine, Kyushu University.

Induction of Colitis

Colitis was induced by intrarectal administration of OXA or TNBS according to the methods described previously.[13,16] Briefly, mice were anesthetized with diethyl ether (Nacalai Tesque, Inc, Kyoto, Japan) and then administered TNBS (3 mg, Sigma-Aldrich Japan Co, Tokyo, Japan) or OXA (0.8% or 1%, 4-ethocymethylene-2-phenyl-2- oxazolin-5-one) (Sigma Chemical Co, St Louis, MO) dissolved in 45% ethanol intrarectally via a 3.5-French catheter equipped with a 1-mL syringe. The catheter was inserted so that the tip was 4 cm proximal to the anal verge, and the haptenating agent was injected with a total volume of 150 μL. To ensure distribution within the entire colon and cecum, mice were held in a vertical position for 30 seconds after the injection. Control mice were administered an ethanol solution without haptenating agent using the same technique.

Histology Assessment of Colitis

The middle parts of colons were removed and fixed with 10% neutral buffered formalin and then embedded in paraffin. After cutting in round slices, the thin tissue sections were stained with H&E. Histology was scored as follows: epithelium (E): 0, normal morphology; 1, loss of globlet cells; 2, loss of globlet cells in large areas; 3, loss of crypts; 4, loss of crypts in large areas; and infiltration (I): 0, no infiltrate; 1, infiltrate around the crypt basis; 2, infiltrate reaching the L muscularis mucosae; 3, extensive infiltration reaching the L muscularis mucosae and thickening of the mucosa with abundant edema; 4, infiltration of the L submucosa.[34] The total histologic score was given as E + I.

Antibodies and Reagents

FITC-conjugated anti-CD3ε, anti-CD4, anti-CD11c, anti-NK (DX5), anti-CD11b, anti-Foxp3, anti-CD25, and anti-IL-10 mAbs; PE-conjugated anti-Ly-6G, anti-CD30L, anti-CD30, anti-CD8α, anti-CD4, anti-CD25, anti-IFN-γ, anti-IL-10, and anti-IL-4 mAbs; allophycocyanin (APC)-conjugated anti-CD3ε and anti-CD44 mAbs; and biotin-conjugated anti-F4/80 (BM8) and anti-CD30L and APC-conjugated streptavidin (SA-APC) mAbs were purchased from e-Bioscience (San Diego, CA). PE-conjugated anti-TCR$\gamma\delta$ (GL-3) mAb and PerCP-Cy5.5-labeled anti-CD4 were purchased from BD PharMingen (San Diego, CA). Armenian Hamster IgG1 was purchased from Wako Pure Chemicals (Osaka, Japan).

In Vivo Treatment of Mice With Abs

Agonistic anti-CD30 mAb (clone 30.1) and rat anti-mouse IL-4 (clone 11B11) mAb were obtained by growing hybridoma cells in CELLine CL-1000 (BD, Biosciences, San Diego, CA) with serum-free medium (medium 101; Nissui Pharmaceutical, Tokyo, Japan) and collecting these antibodies by HiTrap Protein G HP (Amersham Biosciences). The purity of the preparation was confirmed by SDS-PAGE, and the concentration of Ab was determined by the Lowry method. The mAbs, diluted to 1 mg/mL in phosphate-buffered saline (PBS), were stored at −70°C until use. For in vivo neutralization, various doses of rat anti-mouse IL-4 or isotype control (rat IgG; e-Bioscience) were intraperitoneally (IP) injected into mice at the time of disease induction with OXA. For in vivo activation, 100 μg agonistic anti-CD30 mAb or isotype control (hamster IgG1; BD Biosciences) was injected IP into mice before or after induction of colitis.

Flow Cytometry Analysis and Intracellular Cytokine Synthesis Analysis

Lamina propria (LP) cells in the large intestine were isolated by a modified method described previously.[34] LP lymphocytes (LPLs) were purified on a 45%/66.6% discontinuous Percoll (Pharmacia, Uppsala, Sweden) gradient at 600*g* for 20 minutes. For flow cytometry analysis, isolated cells were preincubated with an Fcγ receptor-blocking mAb (CD16/32; 2.4G2) for 15 minutes at 4°C then incubated with saturating amounts of FITC-, PE-, APC-, and biotin-conjugated mAbs for 30 minutes at 4°C. To detect biotin-conjugated mAb, cells were stained with APC-conjugated streptavidin, and the stained cells were analyzed by using a FACS Calibur flow cytometer (Becton Dickinson, Mountain View, CA). For intracellular cytokine staining, 10^6 LP cells were simulated with phorbol myristate acetate (PMA) and ionomycin for 5 hours at 37°C. Brefeldin A (10 μg/mL; Sigma Chemical Co) was included during the final 4 hours of stimulation. These cells were harvested, washed, and incubated for 30 min at 4°C with mAbs for surface staining then cells were

subjected to intracellular cytokine staining using the Fast Immune Cytokine System according to the manufacturer's instructions (Becton Dickinson Co). The data were analyzed with CellQuest software (BD Biosciences).

Culture of LP Cells for Assay of Cytokine Production

To measure cytokine production by LP cells, 10^6 LP cells from mice were cultured without any stimulation for 24 hours at 37°C under 5% CO_2 in 96-well flat-bottomed plates in a volume of 0.2 mL RPMI containing 10% fetal bovine serum (FBS). For cytokine production by LPT cells, LP cells purified as described above were loaded into uncoated culture wells or wells coated with 10 μg/mL anti-CD3ε mAb and 1 μg/mL soluble anti-CD28 mAb and cultured for 48 hours. The culture supernatants were then harvested and assayed for cytokine concentration by enzyme-linked immunosorbent assay (ELISA) using an ELISA Development Kit (Genzyme Diagnostics, Cambridge, MA).

Statistical Analysis

The difference in survival rates was evaluated by the log-rank test (Mantel-Cox). Disease activity index and histologic scores were statistically analyzed using the Mann-Whitney *U* test. Differences in parametric data were evaluated by Student *t* test. Differences of $P < .05$ were considered statistically significant.

Results

CD30LKO Mice Are Susceptible to OXA-Induced Colitis

To examine the role of CD30L in development of OXA-induced colitis in mice, CD30LKO mice with BALB/c background were subjected to induction of colitis by intrarectal administration of 1.0% or 0.8% OXA. We first examined the expression levels of CD30L and CD30 on LPL in the colon from naive mice and mice with colitis. The CD30L was expressed mainly on a part of $CD4^+$ T cells from freshly isolated LPL in naive BALB/c mice and mice treated with 0.8% OXA 4 days previously (see Supplemental Figure 1*A* and 1*B* online at www.gastrojournal.org). Although the CD30 expression was not detected on freshly isolated LPL cells in the colon of naïve mice or OXA-treated mice (data not shown), appreciable numbers of $CD30^+$ cells were detected in the $CD4^+$ T-cell population from naïve and OXA-treated mice after 24-hour in vitro culture with or without anti-CD3 mAb stimulation (see Supplemental Figure 1*C* online at www.gastrojournal.org).

The survival rates were significantly decreased in CD30LKO mice compared with those in WT mice after 1% OXA administration (Figure 1*A*, $*P < .05$). CD30LKO mice showed exacerbated colitis as indicated by the significant weight loss from day 3 to day 10 after 0.8% OXA administration (Figure 1*B*, $*P < .05$). Macroscopic examinations on day 2 after 0.8% OXA administration revealed that the colon was shorter in CD30LKO mice than that in WT mice (Figure 1*C* and 1*D*, $*P < .05$). On histologic examination of involved colon of 0.8% OXA-treated wild-type (WT) mice, we observed a superficial inflammation characterized by the presence of epithelial cell loss and patchy ulceration, pronounced depletion of mucin-producing goblet cells, and reduction of the density of the tubular glands. In addition, in the LP, a mixed inflammatory cell infiltrate consisting of lymphocytes and granulocytes was associated with an exudation of cells into the bowel lumen. These histopathologic changes of OXA-induced colitis were more serious in the colon of CD30LKO mice than in WT mice, and the histologic score of the colon was significantly higher in CD30LKO mice than in WT mice on day 2 after OXA administration (Figure 1*E* and *F*, $*P < .05$). Thus, CD30LKO mice were highly susceptible to OXA-induced colitis compared with control WT mice.

Cell Accumulation in the Colon Mucosa of CD30LKO Mice With OXA-Induced Colitis

Populations of LP cells in the large intestines from CD30LKO mice before and on day 4 after 0.8% OXA administration were analyzed by flow cytometry. As shown in Supplemental Figure 2*A* (see Supplemental Figure 2*A* online at www.gastrojournal.org), the proportions of $CD11b^+Gr\text{-}1^+$ and $CD11b^+F4/80^+$ cells were significantly higher than OXA-treated WT mice ($*P < .05$), whereas the proportions of $\gamma\delta TCR^+CD3^+$ and $DX5^+CD3^-$ cells had slightly decreased in OXA-treated CD30LKO mice compared with OXA-treated WT mice (see Supplemental Figure 2*B* online at www.gastrojournal.org, $*P < .05$ or $**P < .01$). The relative numbers of $CD4^+CD25^+$ and $CD4^+CD44^+$ T cells were significantly lower in CD30LKO mice before or after OXA-administration (see Supplemental Figure 2*C* online at www.gastrojournal.org, $*P < .05$). Intracellular staining analysis for expression of Foxp3 revealed that $CD4^+CD25^+$ T cells were divided into 2 populations on the basis of Foxp3 expression.[35] $CD4^+CD25^+Foxp3^-$ T cells were selectively reduced in CD30LKO mice before and after OXA administration (see Supplemental Figure 2*D* online at www.gastrojournal.org, $*P < .05$). CD30L was expressed by $CD4^+CD25^+Foxp3^-$ T cells but not by $CD4^+CD25^+Foxp3^+$ T cells (see Supplemental Figure 2*D* online at www.gastrojournal.org).

Cytokine Production by LP Cells of CD30LKO Mice With OXA-Induced Colitis

The spontaneous release levels of IFN-γ, TNF-α, IL-12p40, and IL-10 were significantly lower in CD30LKO mice than in WT mice before and on day 4 after 0.8% OXA administration (Figure 2*A*, $*P < .05$ or $**P < .01$), but the levels of IL-1β and IL-6 were significantly higher in CD30L KO mice than in WT mice ($*P < .05$ and $**P < .01$). The secretion of IL-4 and IL-13 were significantly higher, but the levels of IL-10 and IFN-γ were significantly lower in naïve and OXA-treated

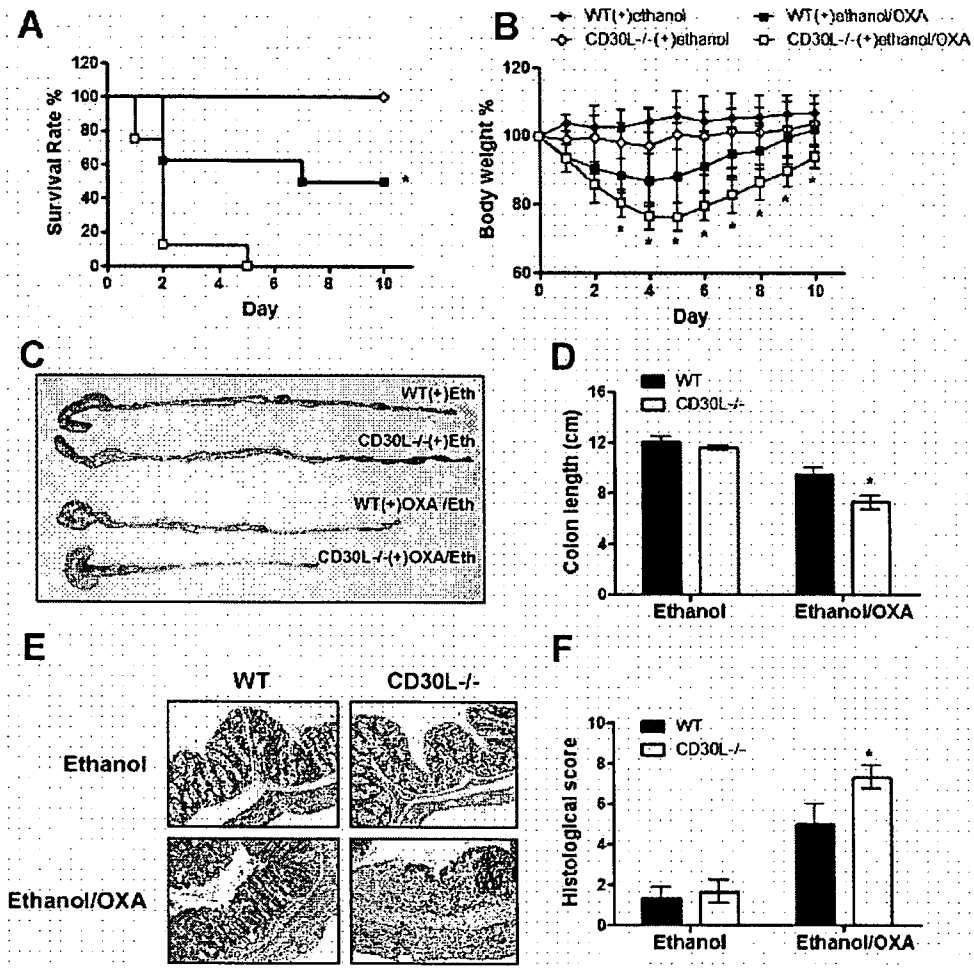

Figure 1. Susceptibility of CD30L$^{-/-}$ mice to OXA-induced colitis. Survival rate (*A*) and weight loss (*B*) of mice after intrarectal administration of 1% or 0.8% OXA, respectively. (*C*) Macroscopic changes of colons on day 2 after administration of 0.8% OXA. (*D*) Colon length measured on day 2 after 0.8% OXA administration. (*E*) Histologic analysis of the colons from mice on day 2 after 0.8% OXA administration (original magnification, ×200). (*F*) Histologic scores of the colons from ethanol- and OXA-treated WT and CD30L$^{-/-}$ mice. Data shown represent mean values ± SD of 24 mice of each group obtained from 3 independent experiments. Statistically significant differences from the value for OXA-treated WT mice are shown (*$P < .05$).

CD30LKO mice than WT mice upon stimulation with anti-CD3/anti-CD28 mAbs (Figure 2*B*, *$P < .05$ or **$P < .01$).

To identify T-cell populations producing IFN-γ, IL-4, or IL-10, we examined intracellular cytokine flow cytometry analysis on LP T cells in OXA-induced colitis. CD4$^+$ T cells were major producers of IL-4 and IL-10 (Figure 3*A* and 3*C*), whereas CD4$^-$ T cells produced an appreciable level of IFN-γ in addition to CD4$^+$ T cells (Figure 3*B*). The absolute numbers of IL-4$^+$CD4$^+$ T cells were significantly higher in naïve and OXA-treated CD30LKO mice than in WT mice (Figure 3*A*, *$P < .05$ or **$P < .01$). The absolute numbers of IFN-γ$^+$CD4$^+$ T cells and IL-10$^+$CD4$^+$ T cells were significantly lower in OXA-treated CD30LKO mice compared with OXA-treated WT mice (Figure 3*B* and *C*, **$P < .01$). We further characterized these CD4$^+$ T cells in the LP of the colon in mice with OXA-induced colitis. IFN-γ was produced mainly by the CD4$^+$CD25$^-$ T-cell population, whereas CD4$^+$CD25$^+$ T cells mainly produced IL-10. CD4$^+$CD30L$^-$ T cells preferentially produced IFN-γ and IL-10 (see Supplemental Figure 2*E* and *F* online at www.gastrojournal.org).

In Vivo Treatment With Anti-IL-4 mAb Ameliorates OXA-Induced Colitis in CD30LKO Mice

To determine the involvement of elevated IL-4 in the pathogenesis of OXA-induced colitis in CD30LKO mice, we examined the effect of in vivo administration of anti-IL-4 mAb on OXA-induced colitis in CD30L KO mice. In vivo injection of more than 0.3 mg anti-IL-4 mAb significantly ameliorated OXA-induced colitis in CD30LKO mice (Figure 4*A–C*, *$P < .05$ or **$P < .01$). The levels of IL-10 and IFN-γ were significantly higher in anti-IL-4 mAb- and OXA-treated CD30LKO mice than in control IgG- and OXA-treated

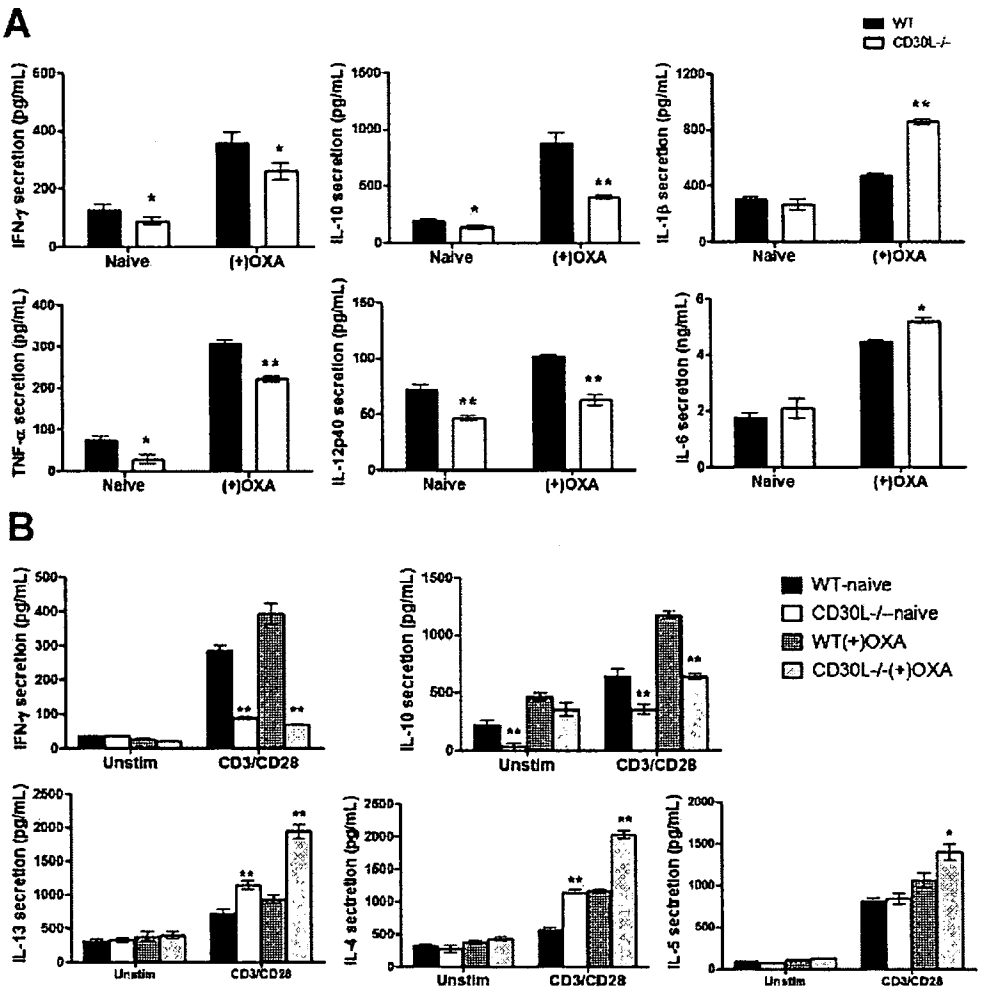

Figure 2. Cytokine production of LP cells in large intestines in OXA-inducted colitis after 24 hours cultured without any stimulation (*A*) and 48 hours cultured with anti-CD3/CD28 mAbs (*B*). Each *column* and *vertical bar* indicates means ± SD for 5 mice of each group. Data of a representative experiment are shown from 3 independent experiments. Statistically significant differences are shown (*$P < .05$ or **$P < .01$).

CD30LKO mice upon stimulation with anti-CD3/anti-CD28 mAbs, (Figure 4*D*, *$P < .05$ or **$P < .01$). IL-13 production was not affected in CD30LKO mice by anti-IL-4 mAb treatment. Similarly, anti-IL-4 mAb treatment ameliorated OXA-induced colitis in WT mice (see Supplemental Figure 3 online at www.gastrojournal.org). Thus, these results suggest that IL-4 is involved in the pathogenesis of OXA-induced colitis in WT and CD30LKO mice.

In Vivo Treatment With Agonistic Anti-CD30 mAb Ameliorates OXA-Induced Colitis in CD30LKO and WT Mice

To elucidate the roles of CD30L/CD30 signaling in OXA-induced colitis, we examined the effect of in vivo administration of agonistic anti-CD30 mAb (CD30.1)[18] on OXA-induced colitis in CD30L KO mice. Mice were injected IP with anti-CD30 mAb or control hamster IgG1 24 hours before 1% OXA administration for survival rate or 0.8 % OXA treatment for weight loss. In vivo injection of anti-CD30 mAb significantly protected against OXA-induced colitis in CD30LKO mice as assessed by both survival rate and weight loss (Figure 5*A*, *$P < .05$ or **$P < .01$). These results suggest that CD30 signaling is important for controlling OXA-induced colitis. The secretion of IL-4 and IL-13 were significantly lower, but the levels of IL-10 and IFN-γ were significantly higher in anti-CD30 mAb- and OXA-treated CD30LKO mice than in control antibody and OXA-treated CD30LKO mice upon stimulation with anti-CD3/anti-CD28 mAbs (Figure 5*B*, *$P < .05$ or **$P < .01$). Thus, these results suggest that stimulating reagent for CD30 signaling may be useful to control OXA-induced colitis.

We further examined the effect of in vivo treatment with agonistic anti-CD30 mAb on OXA-induced colitis in WT mice. Although in vivo treatment with anti-CD30 mAb 1 day after 1.5% OXA administration did not affect

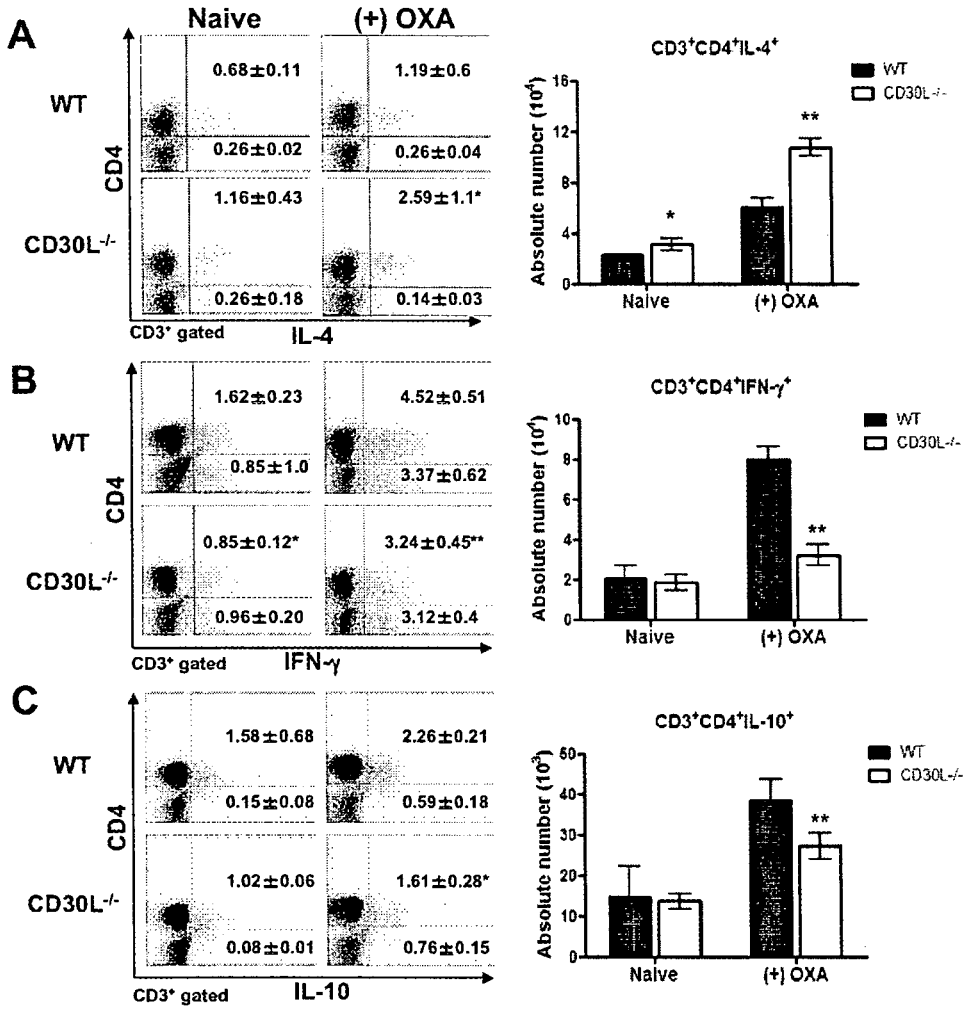

Figure 3. Intracellular cytokine expression by LP T cells from OXA-treated CD30L$^{-/-}$ mice. LP T cells from mice treated with 0.8% OXA 4 days previously were cultured with PMA plus ionomycin and analyzed for the expression of CD4 and IL-4 (*A*), IFN-γ (*B*), or IL-10 (*C*) by intracellular staining. The absolute number of each subset was calculated by multiplying the total number of LP T cells by the percentage of each subset. *Values* of each *column* and *vertical bar* indicate means ± SD for 5 mice within each group. Representative data are shown from 3 independent experiments. Statistically significant differences are shown (*$P < .05$ or **$P < .01$).

OXA-induced colitis, the treatment 1 day before or at the same time as OXA administration significantly extended the survival period and decreased weight loss of WT mice with OXA-induced colitis (Figure 5C, **$P < .01$). Thus, anti-CD30 mAb may be useful as a novel biologic therapy for UC.

CD30LKO Mice Are Resistant to TNBS-Induced Acute Colitis

TNBS-induced acute colitis is thought to be a Th1 cell-mediated inflammation.[11-13] To examine the role of CD30L in development of TNBS-induced acute colitis in mice, we next examined TNBS-induced acute colitis with a Th1-like response in CD30LKO mice with C57BL/6 background. The CD30L was expressed mainly on a part of CD4$^+$ T cells from freshly isolated LPL in naïve C57BL/6 mice and mice treated with TNBS 7 days previously (see Supplemental Figure 1*A* online at www.gastrojournal.org). The CD30 expression on CD4$^+$ T cells from LPL was detected only when the LPLs were cultured in vitro and the level of CD30$^+$ in CD4$^+$ cells were significantly increased in mice with TNBS-induced colitis than naive mice (see Supplemental Figure 1C online at www.gastrojournal.org, *$P < .05$).

As shown in Figure 6*A* and *B*, TNBS-induced acute colitis was attenuated in CD30LKO mice as indicated by survival rate and weight loss (*$P < .05$). Macroscopic inspection showed a significantly longer colon in CD30LKO mice than in WT mice on day 7 after TNBS administration (Figure 6*C*, *$P < .05$). The histologic score of the colon was significantly lower in CD30LKO mice than in WT mice (Figure 6*D*, **$P < .01$).